E. Krempl and H. Lu†*

The Path and Amplitude Dependence of Cyclic Hardening of Type 304 Stainless Steel at Room Temperature

REFERENCE Krempl, E. and Lu, H., **The path and amplitude dependence of cyclic hardening of type 304 stainless steel at room temperature,** *Biaxial and Multiaxial Fatigue*, EGF 3 (Edited by M. W. Brown and K. J. Miller), 1989, Mechanical Engineering Publications, London, pp. 89–106.

ABSTRACT A servohydraulic MTS axial–torsion test system with computer control was used to perform constant amplitude, completely reversed, strain controlled, axial, torsional and ninety degree out-of-phase tests on annealed type 304 stainless steel at room temperature. An Instron biaxial extensometer provided for the biaxial strain measurements. During all tests the effective strain rate was kept constant.

At the same effective strain range, tests with alternating axial and torsional straining showed a higher degree of cyclic hardening than axial or torsional cycling. The results are indicative of the path dependence of cyclic hardening and of a gradually developing cross-effect.

When the effective peak stresses in axial and out-of-phase cycling at different effective strain amplitudes are plotted versus inelastic strain path length, *one* curve is obtained for *each test*. Based on the concept of reversible and irreversible inelastic strain, two new measures akin to the inelastic strain path length are derived and shown to correlate all the data into a single master curve. The new measures correlate the different amplitude data and are intended for use in modeling cyclic in-phase and out-of-phase behaviours in constitutive equations, specifically the viscoplasticity theory based on overstress.

Introduction

Within recent years servo-controlled axial–torsion systems and computer control have become available. When coupled with biaxial extensometers which measure the strain on the uniform section of the specimen (almost invariably a thin-walled tube), there exist unprecedented capabilities of testing, and very interesting results for both the deformation and the fatigue behaviour of materials are becoming available.

It is well known from uniaxial studies that the cyclic inelastic deformation behaviour of metals can be classified as predominantly 'cyclic neutral', 'cyclic hardening', or 'cyclic softening'. This classification is based on the variation of the stress range with cycles under strain controlled loading. The difference in the cyclic and monotonic behaviour is highlighted by the monotonic and the cyclic stress–strain diagrams (**1**). During biaxial in-phase testing in the axial-shear strain space, similar hardening phenomena can be observed which can be correlated successfully by using the second invariants of the stress and the strain

* Department of Mechanical Engineering, Aeronautical Engineering, and Mechanics, Rensselaer Polytechnic Institute, Troy, NY 12181-3590, USA.
† Now with Bendix Corporation, South Bend, IN, USA.

deviator tensors (2)(3) (the so-called von Mises effective stress (strain)). However, when cyclic hardening alloys are subjected to out-of-phase loading, extra hardening is observed (2)–(8), which far exceeds that observed in in-phase loading. The extra hardening depends on the strain path (3)(6)–(8) and on the effective strain amplitude. For alloys which behave in a cyclic neutral fashion, the extra hardening during out-of-phase cycling is insignificant (9)–(11). It is interesting to observe in this context that type 316 stainless steel tested in (3) produced some hardening in in-phase cycling but showed substantial hardening during out-of-phase loading. In contrast, the 6061 T6 Al alloy tested in (9) and the B1900 + Hf alloy investigated in (11) exhibit almost no cycle dependent changes in in-phase and in out-of-phase tests.

In addition to the extra hardening in out-of-phase loading, the stainless steels exhibit a cross-effect when the direction of straining is changed without altering the effective strain range (2)(6)(8). When, after saturation an axial (or torsional) test was conducted following torsional (or axial) cycling, the stress range immediately after the change in direction increased considerably (2). This cross-effect was found to disappear after out-of-phase cycling (2). However, continuous axial or torsional, strain controlled cyclic tests conducted at the same effective strain range gave the same effective stress vs accumulated inelastic strain curves.

Engineering alloys, specifically stainless steels, were shown to exhibit considerable rate (time) dependence of the inelastic deformation at room temperature (12)–(14). If it is assumed that the total stress range consists of time-dependent (viscous) and time-independent (plastic) contributions, it becomes important to know how these contributions change during cycling. (Roughly speaking the viscous contribution to the total stress range is equal to the sum of the relaxation drops at the maximum and the minimum strain in very long relaxation tests, see (24).) Through appropriate check tests it was shown, in (2), that the cyclic hardening of annealed type 304 stainless steel is almost exclusively due to changes in the plastic contribution to the stress. Compared to the observed changes in the stress amplitude the changes in the viscous contribution are negligible.

The properties delineated above are of interest for the modeling of deformation behaviour, i.e., for the constitutive equation development. A knowledge of the inelastic deformation behaviour is very important and a prerequisite for the life prediction of components. It is the purpose of this paper to contribute new information regarding the biaxial deformation behaviour and its correlation for a strongly cyclic hardening alloy, annealed type 304 stainless steel.

Notation

ε_e	Effective total strain, defined in equation (1)
ε	Engineering axial strain
γ	Engineering shear strain
σ_e	Effective peak stress, defined in equation (2)

σ	Axial stress
τ	Shear stress
$\dot{p}$	Rate of inelastic strain path length defined in equation (3)
E, G	Elastic, shear modulus
ε_{ic}	Irreversible plastic strain, defined in equation (4)
ε_r	Reversible plastic strain, defined in equation (5)
n	Number of half cycles, number of reversals
n_s	Number of reversals to saturation
p_{ic}	Irreversible, inelastic strain path length defined in equation (6)
p_s	Inelastic strain path length at saturation
J	A measure to distinguish between in-phase and out-of-phase loading, introduced in equation (7)
Ω	A tensorial measure for non-proportional loading, defined in equation (8)
$\dot{p}_o$	Rate of out-of-phase path length, defined in equation (9)
$\dot{p}_i$	Rate of in-phase path length, defined in equation (10)
$\dot{p}_{il}$	Retarded rate of in-phase path length, defined in equation (15)
$\dot{p}_{ol}$	Retarded rate of out-of-phase path length, defined in equation (16)
$\dot{p}_g$	Rate of combined inelastic path length, defined in equation (17)

Experimental arrangements and test material

The experimental arrangements are fully described in references (**2**)(**10**) and involve tubular specimens with strain measurement on the gauge length via an Instron biaxial extensometer. The testing was done at room temperature with an MTS axial–torsion servohydraulic test system using an MTS 463 Data/Control Processor. Recording of test results was accomplished with *XY* recorders and with digital data acquisition. The testing procedure involved a return to zero stress and strain values under computer control whenever a comparison with other test results generated under identical command wave forms became necessary (**2**).

Type 304 stainless steel from reference heat 9T 2796 was donated by the Department of Energy. The nominal chemical composition as supplied by DOE is (wt %): 0.044 C, 1.26 Mn, 0.033 P, 0.016 S, 0.45 Si, 9.50 Ni, 18.64 Cr, 0.34 Mo, 0.25 Cu. After machining, the tubular specimens (see Fig. 1 of (**9**)) were subjected to a heat treatment of 90 minutes at 2000°F (1093°C) in vacuum, resulting in a 0.2 per cent yield strength of about 180 MPa at a strain rate of 10^{-5} s^{-1}, see (**12**).

Cross-hardening in type 304 stainless steel

In reference (**2**) specimens were strain cycled at a constant effective strain amplitude in tension or torsion until saturation of hardening was achieved. Following a return to zero stress and strain, specimens which were cycled axially (or torsionally) were then subjected to a single torsional (or axial) strain cycle at the same effective strain range. The effective stress range of this single

cycle was invariably greater than the previously attained saturated effective stress range. This result was called the 'cross-effect' and its appearance was something of a surprise since, it implied latent hardening and anisotropy of the cyclic hardening process. Similar results were found in (**6**)(**8**).

The question arises how the cross-effect develops with hardening. To answer it, the following tests were performed at the same effective strain amplitude $\varepsilon_{ea} = 0.008$ obtained from

$$\varepsilon_e = (\varepsilon^2 + \gamma^2/3)^{1/2} \tag{1}$$

with ε and γ denoting the axial strain and engineering shear strain, respectively. In the tests the effective strain rate was equal to $3 \times 10^{-4}\ s^{-1}$. It is computed from equation (**1**) with the strains replaced by the corresponding strain rates. Virgin specimens were subjected to one of the following tests:

(i) continuous axial cycling;
(ii) continuous torsional cycling;
(iii) alternate axial–torsional cycling for one cycle each for a total of twenty cycles. After each cycle, stress and strain are returned to zero.

The results of these tests are plotted in Figs 1 and 2. The axial and the torsional hysteresis loops for test (iii) are given in Figs 1(a) and 1(b), respectively. The evolution of hardening is quite evident.

The effective stress is defined as

$$\sigma_e = (\sigma^2 + 3\tau^2)^{1/2} \tag{2}$$

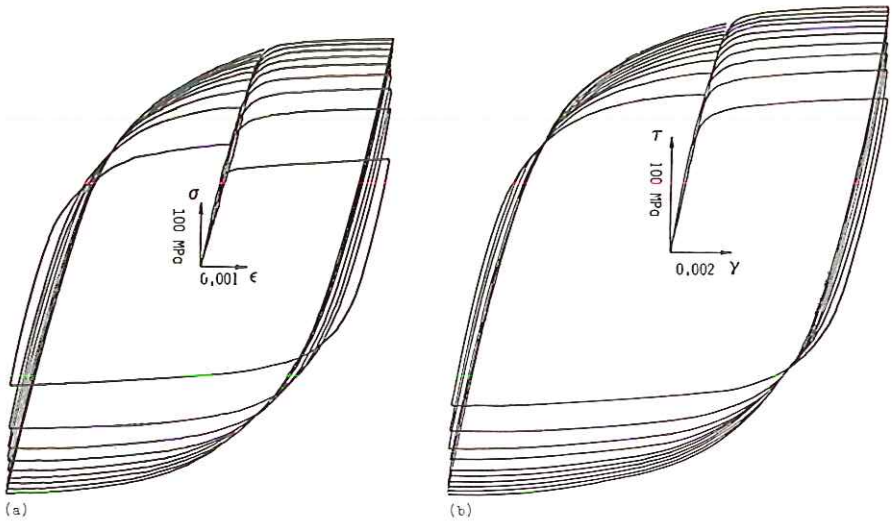

Fig 1 Hysteresis loops for a test with alternate axial/torsion completely reversed cycling with one cycle at each loading mode and subsequent return to zero stress and strain. Effective total strain amplitude $\epsilon_{ea} = 0.008$, effective strain rate $3 \times 10^{-4}\ s^{-1}$. The test starts with axial straining. (a) axial hysteresis loops; (b) torsional hysteresis loops

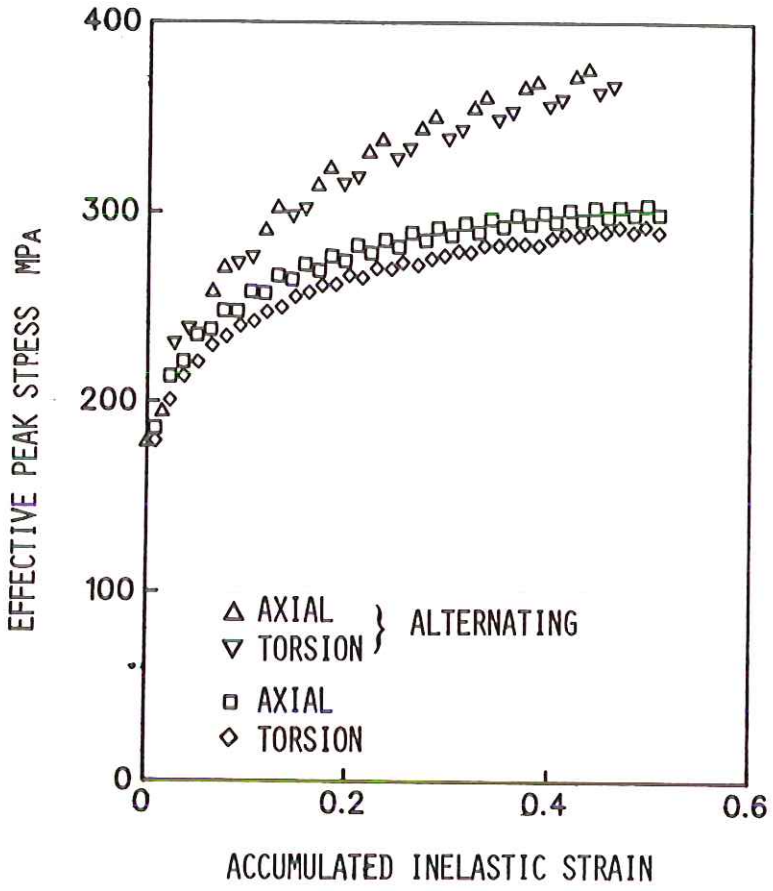

Fig 2 Effective peak stress vs accumulated inelastic strain at $\epsilon_{ea} = 0.008$ with an effective strain rate of $3 \times 10^{-4}\,s^{-1}$. Alternate axial/torsional cycling (see Fig. 1) and continuous axial or torsional cycling

In Fig. 2 the effective peak stress (obtained from equation (2) by inserting peak values of the axial stress (σ) or shear stress (τ)) is plotted vs p, the inelastic strain path length obtained by integration of

$$\dot{p} = \{(\dot{\varepsilon} - \dot{o}/E)^2 + (\dot{\gamma} - \dot{t}/G)^2/3\}^{1/2} \tag{3}$$

A superposed dot indicates the time derivative of the quantity, and E and G designate the elastic modulus and the shear modulus, respectively. It is evident from Fig. 2 that the peak stresses for tests (i) and (ii) are close together, with those of test (iii) are significantly greater. The direction-of-straining changes enhance cyclic hardening considerably. Figure 2 shows that the difference in hardening behaviour develops gradually. It attests to the path dependence of cyclic hardening. The final difference between the peak stresses in tests (i), (ii),

and (iii) is approximately 70 MPa. The cross-effect in axial–torsion is between 40 and 60 MPa, see Table 2 of (**2**). It is further amplified by cyclic hardening before softening sets in, see Fig. 4 of (**2**) after the first segment.

In Fig. 2 the effective peak stress correlates the axial and the torsion tests reasonably, but not perfectly. The axial values are consistently higher than the torsional values in tests with and without a change in direction.

The different cyclic hardening behaviour of test (iii) can be rationalized by considering that the plane of maximum shear strain (maximum slip) changes with the direction of straining. In test (iii) twice as many such planes are operative than in tests (i) or (ii). The potential for dislocation movement, multiplication, and interaction is, therefore, increased in the test with alternating axial–torsional straining.

If this explanation is adopted the magnitude of the cross-effect reported in (**2**) is puzzling. In these tests the direction of straining is not changed until saturation is reached; therefore, certain slip directions are not activated. A single cycle which activates these 'dormant' slip directions produces almost as much hardening as the stress difference between the tests with and without change in direction of straining (see Fig. 2). Latent hardening must be present to explain this observation. Hardening is then intensified for a few cycles (further hardening is observed) before softening sets in (see Fig. 4 of (**2**)).

It is also obvious that the saturated value of the peak stress depends on the type of test. Extrapolated values are about 330 MPa for the tests with no change in direction, and about 400 MPa for test (iii). For 90 degree out-of-phase loading, the hardening is stronger than in any of the tests reported in Fig. 2. In this case the saturated value of the effective stress is considerably above 550 MPa (**10**). Therefore, cyclic hardening from the annealed state is strongly dependent on the strain path. It appears that 90 degree out-of-phase cycling generates the most hardening.

The testing procedure in (**2**) was such that, after each constant amplitude cycling to saturation, check tests were performed followed by a change in direction of cyclic straining. The cross-effect was found, i.e., an increase in effective stress amplitude *after a change in direction*. When cycling continued in a different direction a short period of further hardening was followed by considerable softening. The question arises whether the cross-effect and softening would still be observed if after the check tests *cycling continues without a change in direction*. Therefore, a torsional cyclic test with the same subsequent checks as in (**2**) was performed (the first check was always in the direction of previous cycling if axial or torsional cycling was used).

The results are shown in Fig. 3. The peak effective stresses observed during torsional checks, which were performed before the axial checks, and are represented by filled triangles, are very close to the corresponding torsional continuous cycling peak stresses. The subsequently obtained axial effective peak stresses, represented by open triangles, are always higher than those

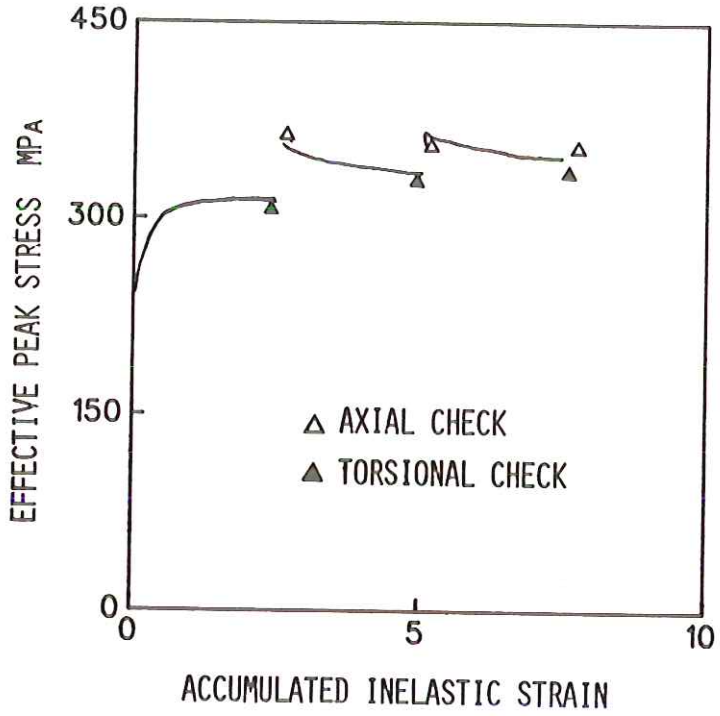

Fig 3 Effective peak stress versus accumulated inelastic strain for completely reversed, strain controlled torsional cycling interrupted by torsional (filled triangles) and axial (open triangles) check tests. Each test starts from zero stress and strain. $\epsilon_{ea} = 0.008$, effective strain rate $3 \times 10^{-4}\,s^{-1}$

obtained in torsion and represent the cross-effect. It diminishes with accumulated inelastic strain. Surprisingly, after the axial check tests, the torsional stress amplitude commences at the stress level of the axial check test (no further cross-effect), softening sets in and continues with a decreasing rate.

It is obvious from Fig. 3 that the cross-effect and the subsequent softening are due to a single cycle in the axial direction. It is also noteworthy that, after the single axial cycle is followed by torsional cycling, no additional cross-effect is observed. The single axial cycle must have hardened the torsional slip systems so that they can support the high stress amplitude.

In Fig. 3 torsional cycling was not continued long enough to obtain a steady-state condition. It appears that, after the changes in direction, a higher effective steady-state stress amplitude would be attained than in continuous cycling without a change in direction.

The cross-effect and the softening, after a change in direction, of the otherwise hardening material provide a great challenge for constitutive modelling.

Correlation of results obtained in in-phase and out-of-phase cycling

Background

In classical time-independent plasticity theory, cyclic hardening is modelled by letting the yield surface expand uniformly. The size of the yield surface is made to depend on either the accumulated inelastic strain or on plastic work. Both of these measures have the properties that they are only zero when the deformation is always linearly elastic and that they do not decrease with deformation. The use of these quantities is interchangeable in conventional plasticity.

Experiments on engineering alloys have shown that inelastic deformation is rate (time) dependent at ambient temperature (**2**)(**12**)–(**16**). Since this observation is contrary to the assumptions of the classical theories, the assumption of using inelastic work or accumulated inelastic strain path lengths for the modelling of cyclic hardening was checked by suitable experiments in (**13**). They showed that inelastic work was not a suitable quantity, but did not rule out the use of the inelastic strain path length, or any other quantity which was not in conflict with the experimental evidence.

In low-cycle fatigue testing, the progression of the cycle dependent changes is usually plotted against the number of cycles. The drawback in this way of plotting is that it is only useable for the case of periodic loading. For constitutive modelling, an invariant quantity which, would be applicable for any kind of loading, is preferred. Such a quantity is the inelastic strain path length, p, obtained by integrating equation (3). Whereas cycles are a strictly increasing quantity, the inelastic strain path length is non-decreasing. However, this minor difference is not important, and the results are plotted with the quantity p as 'abscissa'.

Experimental results

In Fig. 4 the peak stress of uninterrupted uniaxial tests at two strain ranges are plotted against accumulated inelastic strain path length, together with the effective stress in out-of-phase loading at three different effective strain ranges. The effective strain rate is $3 \times 10^{-4}\ s^{-1}$ for all cyclic loadings. The solid line represents the true stress of a tensile test with strain rate cycling between 1.5×10^{-3} and $1.5 \times 10^{-5}\ s^{-1}$.

It is evident from Fig. 4 that the quantity p does not correlate the data at all (a quantity suitable for correlation of the data should compress them into one master curve). For each test a separate curve is obtained. Moreover, at the same effective strain range, uniaxial and out-of-phase loadings proceed along different curves. It is concluded that p is not a very useful measure of hardening in cases where different amplitudes and different types of loadings are involved. The same conclusion is reached in Fig. 10 of (**3**) for type 316 stainless steel (see also the remark on page 290 of (**3**) regarding the use of inelastic work instead of p). In (**2**), specifically Fig. 4, effective stress amplitudes obtained at the *same*

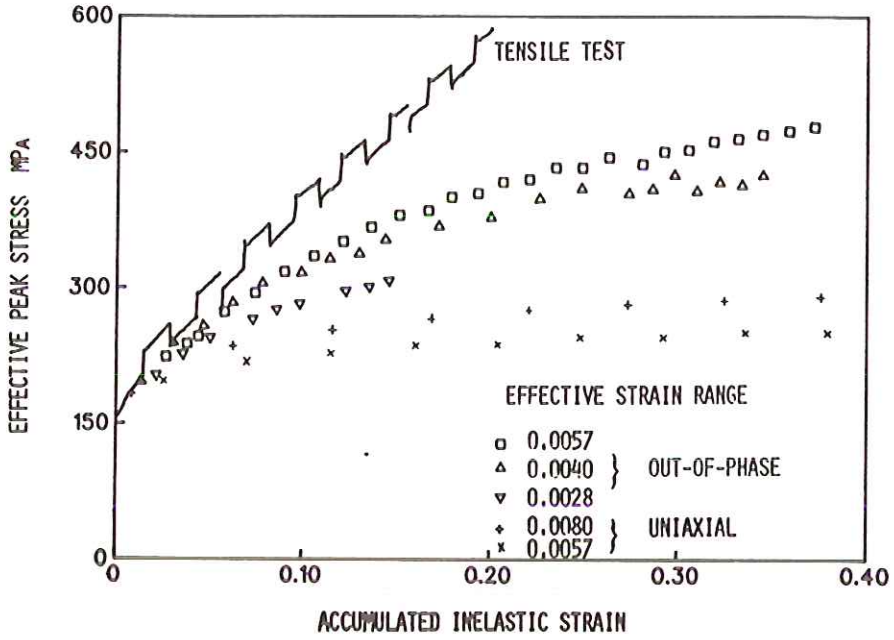

Fig 4 True effective stress (for uniaxial monotonic loading with strain rate cycling between 1.5×10^{-3} and 1.5×10^{-5} s^{-1}), effective stress amplitude (uniaxial, completely reversed, strain controlled cycling at two amplitudes) and effective stress in 90 degree out-of-phase cycling (three amplitudes) versus accumulated inelastic strain path length. The effective strain rate is 3×10^{-4} s^{-1} in all cyclic tests

effective strain amplitudes *correlated very well* the axial, torsional, and in-phase data, but not the out-of-phase data, when plotted against p. It appears that p ceases to be useful when data at different amplitudes or other than proportional loadings are being compared.

Two new measures of hardening

In principle there are two possibilities for obtaining a correlation of the data in Fig. 4. One can introduce a new ordinate. Since the effective stress correlates monotonic and cyclic axial, torsional, and in-phase data very well (2), this possibility was not pursued further.

If the effective stress is maintained as an ordinate, and if new measures for the abscissa are sought, then such new measures should have the following properties:

(i) amplitude dependent compression of the abscissa (relative to p used in Fig. 4);
(ii) stoppage of growth when saturation is reached (If growth would continue at saturation no unique curve could be obtained. Rather several parallel

curves pertaining to different amplitudes would result at high number of cycles.);

(iii) differentiation between proportional and non-proportional loading;

(iv) Invariance, so that it can be applied to any type of loading;

(v) predominantly increasing.

In this study we propose two such measures of hardening, discussed below.

(1) A measured based on microstructural considerations

In the materials science oriented papers the concept of reversible and irreversible plastic strains is introduced (**17**)–(**19**). Reversible plastic strain is found under saturated conditions, when the hysteresis loop is traced over at each cycle. The irreversible plastic strain is negligible under these conditions, but accumulates up to this point. It is thought to be a measure of the net increase in the density of obstacles impeding dislocation motion (**17**). The accumulated irreversible plastic strain, ε_{ic}, is given as (**17**)(**18**).

$$\varepsilon_{ic} = 2n\varepsilon_a - \sum_{i=1}^{n} \varepsilon_r \tag{4}$$

with n denoting the number of half-cycles. The plastic strain amplitude and the absolute value of the reversible plastic strain are ε_a and ε_r, respectively. Following (**19**), the reversible plastic strain can be computed from

$$\varepsilon_r = \left\{2 - \exp\left(-\frac{C(n-1)}{n_s - 1}\right)\right\}\beta \tag{5}$$

where C and β are material constants and n_s is the number of reversals to saturation. Using this formula the results of tensile and cyclic tests were correlated very well (see Figs 1 and 2 of (**19**)).

The measure proposed in equations (4) and (5) is not invariant and cannot be used in other than a uniaxial state of stress. However, it served as a basis for the following invariant measure,

$$dp_{ic} = \left(1 - 1/2\left[1 - \exp\left\{\frac{-Bp}{(1-J)p_s}\right\}\right]\{2 - \exp(-10Cp/p_s) - \exp(-Cp/p_s)\}\right) dp \tag{6}$$

Subscripts ic and s refer to the irreversible and the saturated conditions, respectively. The quantity J is defined in (**7**) and accounts for the effects of out-of-phase loading; B and C are constants. The quantity J switches between $J = 1$ for in-phase loading and $J = 0$ for 90 degree out-of-phase loading. The measure proposed in equation (6) satisfies the conditions given above. Moreover, equation (6) is such that $dp_{ic} = dp$ initially when $p = 0$. The constants B and C are chosen such that $dp_{ic} = 0$ when $p \gg p_s$.

Table 1 gives the data for the tests of Fig. 4 and the values for p_s, as well as

Table 1 Strain histories of annealed specimens of AISI Type 304 stainless steel

Test conditions	*Specimen No.*	$\Delta\varepsilon_t$ (%)	p_s
Out-of-phase straining sine-wave	6	1.14	0.75
	9	0.80	0.5
	10	0.56	0.3
Axial cyclic straining*	1	1.60	0.5
	8	1.14	0.25
Monotonic straining	Bar 1	–	–
Torsional cyclic straining*	2	1.60	0.52

p_s denotes the value of p at saturation under cyclic loading. Since saturation was not reached in out-of-phase straining, p_s was determined using extrapolation.

B = 8; C = 4 obtained from Fig. 3 of (**19**).

$\dot{\varepsilon}_t = 3 \times 10^{-4}\,s^{-1}$ except for Bar No. 1, where strain cycling between 1.5×10^{-3} and 1.5×10^{-4} was performed.

* Triangular wave.

the values for B and C. With these values, equation (6) is numerically integrated using the digitised data of the tests. The correlation shown in Fig. 5 is quite acceptable.

(*2*) *A measure based on continuum mechanics*
Consider the quantity

$$\mathbf{C} = \mathbf{AB} - \mathbf{BA} \tag{7}$$

where **A** and **B** are second-order tensors. If **A** and **B** are collinear or proportional (i.e., $\mathbf{A} = \alpha\mathbf{B}$ where α is a number), $\mathbf{C} = 0$. Such a measure can be useful in distinguishing between proportional and non-proportional loading.

The measure to be constructed should serve the same role as the inelastic strain path length, p. It should be an invariant which is zero at the beginning of inelastic deformation, non-decreasing, and a rate-independent measure, since cyclic hardening was shown to be predominantly plastic (**2**). (If, for a different material, experiments show otherwise, this condition must be changed.)

It is known that during proportional (in-phase) loading the inelastic strain and strain are collinear. When non-proportional (out-of-phase) loading is applied, the direction of inelastic strain and strain rate can be different. We, therefore, propose as a measure of non-proportional loading

$$\Omega = \varepsilon^{in}\dot{\varepsilon}^{in} - \dot{\varepsilon}^{in}\varepsilon^{in} \tag{8}$$

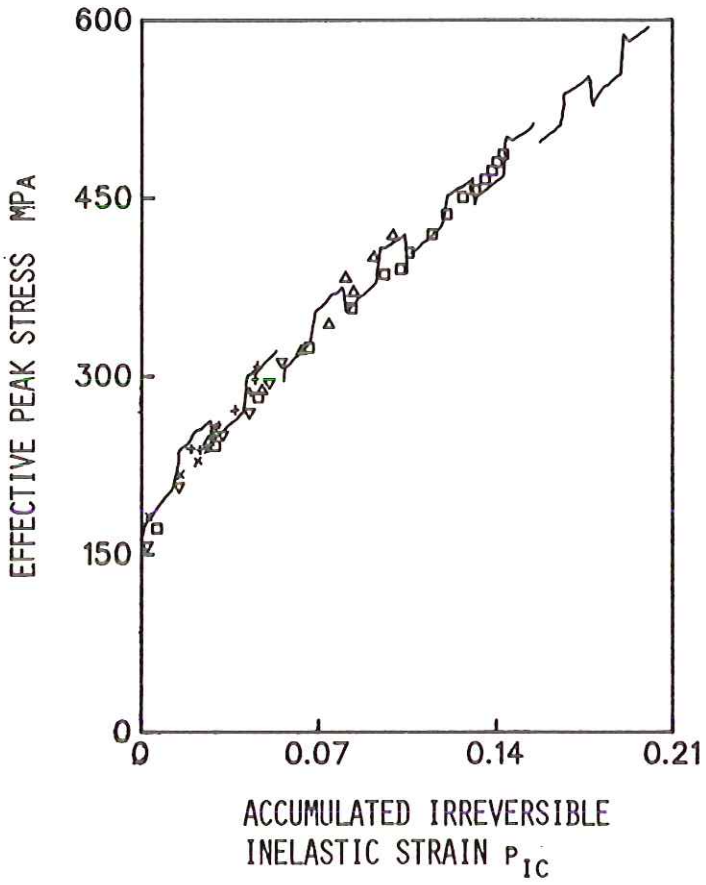

Fig 5 Replot of the data of Fig. 4 using the irreversible accumulated inelastic strain based on microstructural considerations as defined in equation (6). Symbols are identified in Fig. 4

and

$$\dot{p}_o = (\mathrm{tr}\Omega\Omega^T)^{1/2} \tag{9}$$

where tr indicates the trace of a tensor, and the superposed T denotes transpose.

Whenever the inelastic strain and strain rates are collinear, p_o is zero (this happens predominantly in proportional loading). It is, therefore, necessary to find a measure akin to p_o which will also accumulate in proportional loading. A suitable quantity is

$$\dot{p}_i = (\mathrm{tr}\varepsilon^{in}\dot{\varepsilon}^{in}\dot{\varepsilon}^{in}\varepsilon^{in})^{1/2} \tag{10}$$

For the case of the thin-walled tubes used in the present study the inelastic strain and strain rate are given, respectively, by

$$\varepsilon^{in} = \begin{bmatrix} \varepsilon^{in} & \frac{1}{2}\gamma^{in} & 0 \\ \frac{1}{2}\gamma^{in} & -\frac{\varepsilon^{in}}{2} & 0 \\ 0 & 0 & -\frac{\varepsilon^{in}}{2} \end{bmatrix} \tag{11}$$

and

$$\dot{\varepsilon}^{in} = \begin{bmatrix} \dot{\varepsilon} & \frac{1}{2}\dot{\gamma}^{in} & 0 \\ \frac{1}{2}\dot{\gamma}^{in} & -\frac{\dot{\varepsilon}^{in}}{2} & 0 \\ 0 & 0 & -\frac{\dot{\varepsilon}^{in}}{2} \end{bmatrix} \tag{12}$$

Substitution of (11) and (12) into (9) and (10) yields the pertinent expressions as

$$\dot{p}_o = 2[-9/4\varepsilon^{in}\dot{\varepsilon}^{in}\gamma^{in}\dot{\gamma}^{in} + 9/8\varepsilon^{in^2}\dot{\gamma}^{in^2} + 9/8\gamma^{in^2}\dot{\varepsilon}^{in^2}]^{1/2} \tag{13}$$

$$\dot{p}_i = [9/8\dot{\varepsilon}^{in^2}\varepsilon^{in^2} + 5/16\dot{\gamma}^{in^2}\varepsilon^{in^2} + 5/16\gamma^{in^2}\dot{\varepsilon}^{in^2} + 1/8\dot{\gamma}^{in^2}\gamma^{in^2} + 1/8\varepsilon^{in}\dot{\varepsilon}^{in}\gamma^{in}\dot{\gamma}^{in}]^{1/2} \tag{14}$$

The above definitions serve to distinguish between proportional and non-proportional loading. These new strain-path-like parameters must now be used to correlate the data given previously. A retardation feature needs to be introduced to obtain the equivalent of p_{ic} of equation (6). Therefore

$$\dot{p}_{il} = \dot{p}_i \exp(-ap_i) \tag{15}$$

and

$$\dot{p}_{ol} = \dot{p}_o \exp(-bp_o) \tag{16}$$

where a and b are suitable constants. Finally

$$\dot{p}_G = c\dot{p}_{ol} + d\dot{p}_{il} \tag{17}$$

where p_G is now the combined inelastic path length that replaces the inelastic strain path length, p, and where c and d are two additional constants.

With these definitions the previously given data are reanalysed and p_G is determined. The results are plotted in Fig. 6. It is seen that the new combined inelastic path length, p_g, correlates the data very well with the exception of the uniaxial data. (Only one stress–strain curve pertaining to one strain rate is plotted in this figure for clarity.) In correlating the data the constants c and d were set equal to one, and a = 10 000, b = 1000. It is believed that correlation

could be improved by a second analysis of the data. For the moment, the feasibility of this new measure is sufficiently demonstrated.

Discussion

Cross-hardening

The cross-hardening observed in this paper is an effect associated with anisotropy. (Although the same words are used here and in (**20**), the phenomena are different. In (**20**) cross-hardening refers to the additional hardening in out-of-phase loading compared to that in in-phase loading.) Assume that a yield surface is defined at an offset strain equal to the effective strain amplitude. When the direction of straining is changed, the effective stress cannot exceed the one obtained previously if a combination of kinematic and isotropic hardening is assumed. However, the experimental results reproduced in Figs 1–3 of this paper and in Fig. 4 of (**2**) show that this is the case. A distortion of the yield surface must, therefore, be present.

From Fig. 2 it is apparent that the cross-hardening develops gradually in repeated tests. The results of Fig. 3 which show the strong influence of one perpendicular cycle after saturation has been reached are surprising. A single axial cycle increases the effective torsional stress amplitude from approximately 355 MPa to 410 MPa, an increase of roughly 13 per cent. It is concluded that cross hardening is latent. The latent hardening is not stable, it is relieved by subsequent cyclic softening; see Figs 3 and 4 of (**2**). At the same straining direction the cross-hardening phenomenon appears to be temporary, whereas the regular cyclic hardening is permanent.

Although an anisotropic yield function is introduced in (**26**), it is applied to modelling the extra hardening rather than the cross-effect, which is also observed in 316 stainless steel. The time-independent theory proposed in (**8**) permits the modelling of a cross effect for the yield surfaces.

The new measures of hardening

In presently proposed constitutive models, the inelastic strain path length is most frequently used in modelling the isotropic growth of the yield surface. It is also employed in the growth laws for the kinematic variable and for the memory surface (**6**)(**20**)(**22**)(**25**)(**26**). For the modeling of the extra hardening in out-of-phase loading, new scalar (**7**)(**20**) or tensor variables (**26**) are introduced. While success of modelling has been demonstrated at one effective strain amplitude, a correlation for variable effective amplitudes and for different strain paths as shown in Figs 4–6 is not known to the authors.

The measures of hardening proposed here are different from classical notions and stop growing when saturation is reached. This feature was introduced using ideas documented in the materials science literature (**17**)–(**19**).

The two new measures are intended for implementation in the viscoplasticity theory based on overstress (**23**)(**24**). Specifically, they will be used in formulat-

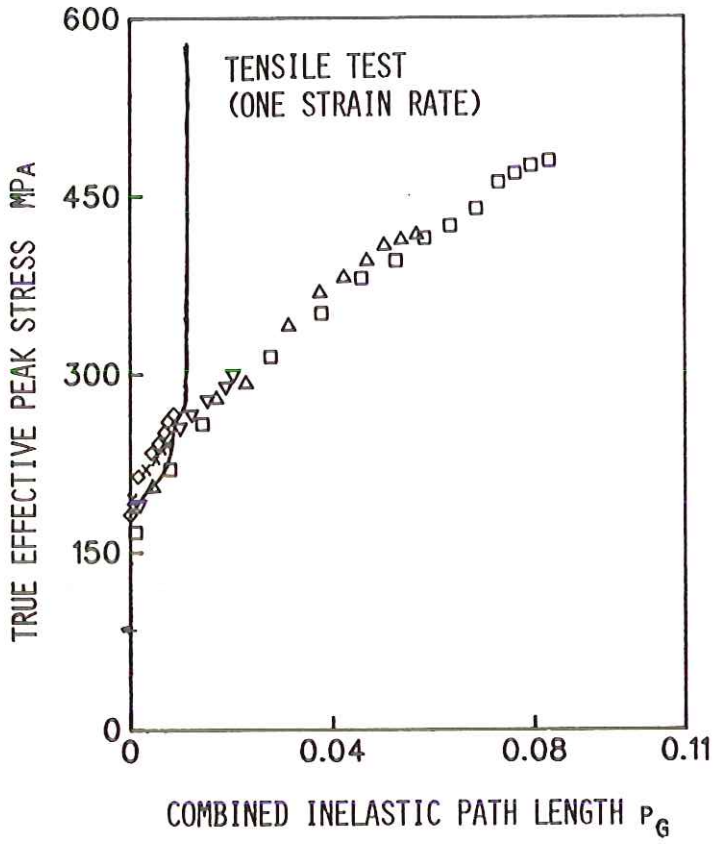

Fig 6 Replot of the data of Fig. 4 using the tensorial invariant defined in equation (17). Symbols are identified in Fig. 4. Data for torsional cyclic loading and identified by (◇) are plotted in addition (the effective strain amplitude is 0.016)

ing a growth law for the quantity A of (23)(24) (see Fig. 1 of (23) for a definition of A) which constitutes the time-independent, asymptotic contribution to the stress. This method of modelling of cyclic hardening is suggested by the room temperature test results obtained on stainless steel (2). If experiments show that cycling causes a change of the viscous contribution to the stress, the viscosity function, k, of (23)(24) must be made to change with cyclic history. It appears that a dependence on the inelastic strain path length can suffice unless there is a marked difference in the viscous contributions to the stress in in-phase and out-of-phase cycling. This property must be ascertained by suitable check tests such as used in (2).

Comparison of Figs 5 and 6 shows a slightly better correlation for the measure based on microstructural considerations and given in equation (6), which will be referred to as 'M1' in the sequel. To differentiate between

in-phase and out-of-phase loading, the quantity J of (7)(20) was included. In the computation of this quantity, an eigenvalue problem in strain space must be solved. The same is true for the measure proposed in (21).

The measure based on equation (17), to be called 'M2', can be directly computed from the inelastic strain and strain rate and involves only matrix operations.

When determined from experimental data, the minimum and maximum shear strains (strain rates) are readily available. The inelastic strain and strain rate needed for M2 require computations of differences, see equation (8). In this case M1 is advantageous. The situation is reversed when the measures are used in computation. The determination of the eigenvalues, and the checking of the 'if' condition necessary for M1, create extra computational effort. The ingredients of M2 are readily available at every time step.

The measure M2 has the possibility of reproducing further hardening upon an increase in strain amplitude once saturation has been reached at a small strain amplitude due to the dependence on the inelastic strain. This has been demonstrated in (27).

It is possible to define the tensor, Ω, and the in-phase rate of path length p_i differently. The inelastic strain in equations (8) and (10) is replaced by the deviatoric equilibrium stress $\mathbf{g}^d$ used in (23). During out-of-phase loading the inelastic strain rate and the deviatoric equilibrium stress are not collinear and Ω is, therefore, non-zero. If this measure is adopted, Ω and p_i are related to the time-independent, plastic work. This property has attractive features which need to be explored together with the mathematical consequences of the use of these new measures in constitutive equations.

The measures introduced in this paper could also be adopted in other theories if it is desired to model amplitude dependence and differences between in-phase and out-of-phase cycling.

Conclusions

The test results show the path dependence of hardening at the same effective strain amplitude and the gradual development of the cross-effect.

The inelastic strain path length is not able to correlate the amplitude dependence of cyclic hardening in uniaxial or in 90 degree out-of-phase loading. Also, at the same effective strain amplitude uniaxial and 90 degree out-of-phase hardening curves are not correlated by the inelastic strain path length.

Two new measures of path length are introduced which are shown to correlate the amplitude and path-dependence of cyclic hardening. One measure is based on microstructural considerations; the other is based on continuum mechanics. The pros and cons of their use in constitutive equations are discussed. The measure based on continuum mechanics reproduces in a natural way further cyclic hardening upon increase of the strain amplitude after saturation at the low amplitude.

Acknowledgement

The support of the Solid Mechanics Program of the National Science Foundation made this research possible. The Department of Energy donated the test material, and Mr E. J. Tracey of the General Electric Company performed the heat treatment.

References

(1) LANDGRAF, R. W., MORROW, J. D., and ENDO, T. (1979) Determination of the cyclic stress–strain curve, *J. Mater.*, **4**, 176–188.
(2) KREMPL, E. and LU, H. (1984) The hardening and rate-dependent behavior of fully annealed AISI type 304 stainless steel under biaxial in-phase and out-of-phase strain cycling at room temperature, *J. Engng Mater. Technol.*, **106**, 376–382.
(3) OHASHI, Y., TANAKA, E., and OOKA, M. (1985) Plastic deformation behavior of type 316 stainless steel subject to out-of-phase strain cycles, *J. Engng Mater. Technol.*, **107**, 286–292.
(4) LAMBA, H. S. and SIDEBOTTOM, O. M. (1978) Cyclic plasticity for nonproportional paths: Part 1 – cyclic hardening, erasure of memory, and subsequent strain hardening experiments, *J. Engng Mater. Technol.*, **100**, 96–103.
(5) KANAZAWA, K., MILLER, K. J., and BROWN, M. W. (1979) Cyclic deformation of 1% Cr–Mo–V steel under out-of-phase loads, *Fatigue Engng Mater. Structures*, **2**, 217–228.
(6) NOUAILHAS, D., POLICELLA, H., and KACZMAREK, H. (1983) On the description of cyclic hardening under complex loading histories, *Constitutive Laws for Engineering Materials/Theory and Application*, Proceedings of the International Conference (Edited by DESAI, C. S. and GALLAGHER, R. H.), pp. 125–132.
(7) McDOWELL, D. L. (1983) On the path dependence of transient hardening and softening to stable states under complex biaxial cyclic loading, *Constitutive Laws for Engineering Materials/ Theory and Application*, Proceedings of the International Conference (Edited by DESAI, C. S. and GALLAGHER, R. H.), pp. 125–132.
(8) ROUSSET, M. (1985) Surface Seuil de Plasticité. Determination Automatique et Modelisation, Report from Laboratoire de Mécanique et Technologie, ENSET, Cachan, France.
(9) KREMPL, E., and LU, H. (1983) Comparison of the stress responses of an aluminum alloy tube to proportional and alternate axial and shear strain paths at room temperature, *Mechanics Mater.*, **2**, 183–192.
(10) LU, H. (1985) *An experimental study of biaxial inelastic deformation behavior of engineering alloys in support of viscoplasticity theory and life prediction*, PhD thesis, Renssalaer Polytechnic Institute, NY.
(11) LINDHOLM, U. S., CHAN, K. J., BODNER, S. R., WEBER, R. M., WALKER, K. P., and CASSENTI, B. N. (1985) Constitutive modeling for isotropic materials (HOST), (Second Annual Status Report), NASA CR 174980.
(12) KREMPL, E. (1979) An experimental study of room-temperature rate sensitivity, creep and relaxation of Type 304 stainless steel, *J. Mech. Phys Solids*, **27**, 363–375.
(13) KREMPL, E. and KALLIANPUR, V. V. (1984) Some critical uniaxial experiments for viscoplasticity at room temperature, *J. Mech. Phys Solids*, **32**, 301–314.
(14) JORDAN, E. H. and FREED, A. D. (1982) Room-temperature post-yield creep, *Expl Mech.*, **22**, 354–360.
(15) KUJAWSKI, D., KALLIANPUR, V., and KREMPL, E. (1980) An experimental study of uniaxial creep, cyclic creep and relaxation of AISI Type 304 stainless steel at room temperature, *J. Mech. Phys Solids*, **28**, 129–148.
(16) KUJAWSKI, D. and KREMPL, E. (1981) The rate (time)-dependent behavior of Ti-7Al-2Cb-1Ta titanium alloy at room temperature under quasi-static monotonic and cyclic loading, *J. appl. Mech.*, **48**, 55–63.
(17) SLEESWYK, A. W., JAMES, M. R., PLANTINGA, D. H., and MAATHUIS, W. S. T. (1978) Reversible strain in cyclic plastic deformation, *Acta Met.*, **26**, 1265–1271.
(18) DANIEL, R. C. and HORNE, G. T. (1971) Bauschinger effect and cyclic hardening in copper, *Met. Trans*, **2**, 1161–1172.

(19) JAMES, M. R. and SLEESWYK, A. W. (1978) Influence of intrinsic stacking fault energy on cyclic hardening. *Acta Met.*, **26**, 1721–1726.
(20) McDOWELL, D. L. (1985) A two surface model for transient nonproportional cyclic plasticity, Parts 1 and 2, *J. appl. Mech.*, **52**, 298–308.
(21) BROWN, M. W. and MILLER, K. J. (1979) Cyclic deformation of 1 percent Cr–Mo–V steel under out-of-phase loads, *Fatigue Engng Mater. Structures*, **2**, 217–228.
(22) CHABOCHE, J. L., DANG VAN, K., and CORDIER, G. (1979) Modelization of the strain memory effect on the cyclic hardening of 316 stainless steel, *Proc. 5th Int. Conf. on Structural Mechanics in Reactor Technology*, Commission of the European Communities and North Holland, Paper L11/3.
(23) YAO, D. and KREMPL, E. (1985) Viscoplasticity theory based on overstress. The prediction of monotonic and cyclic proportional and nonproportional loading paths of an aluminum alloy, *Int. J. Plasticity*, **1**, 259–274.
(24) KREMPL, E., McMAHON, J. J., and YAO, D. (1986) Viscoplasticity based on overstress with a differential growth law for the equilibrium stress, *Mech. Mater.*, **5**, 35–48.
(25) OHNO, N. (1982) A constitutive model of cyclic plasticity with a nonhardening strain region, *J. appl. Mech.*, **49**, 721–727.
(26) NOUAILHAS, D., CHABOCHE, J. L., SAVALLE, S., and CAILLETAUD, G. (1985) On constitutive equations for cyclic plasticity under nonproportional loading, *Int. J. Plasticity*, **1**, 317–330.
(27) YAO, D. (1987) *Theory of viscoplasticity based on overstress with applications*, PhD thesis, Rensselaer Polytechnic Institute, NY.